Influence of CO_2 on the corrosion behaviour of 13Cr martensitic stainless steel AISI 420 and low-alloyed steel AISI 4140 exposed to saline aquifer water environment

A. Pfennig[1] & A. Kranzmann[2]
[1]*FHTW University of Applied Sciences Berlin, Germany*
[2]*BAM Federal Institute of Materials Research and Testing, Germany*

Abstract

The CCS technique involves the compression of emission gasses in deep geological layers. To guarantee the safety of the site, CO_2-corrosion of the injection pipe steels has to be given special attention when engineering CCS-sites. To get to know the corrosion behaviour samples of the heat treated steel AISI 4140, 42CrMo4, used for casing, and the martensitic stainless injection-pipe steel AISI 420, X46Cr13 were kept at T=60°C and p=1-60 bar for 700 h-8000 h in a CO_2-saturated synthetic aquifer environment similar to the geological CCS-site at Ketzin, Germany. The isothermal corrosion behaviour obtained by mass gain of the steels in the gas phase, the liquid phase and the intermediate phase gives surface corrosion rates around 0.1 to 0.8 mm/year. Severe pit corrosion with pit heights around 4.5 mm are only located on the AISI 420 steel. Main phase of the continuous complicated multi-layered carbonate/oxide structure is siderite $FeCO_3$ in both types of steel.

Keywords: steel, pipeline, corrosion, carbonate layer, CCS, CO_2-injection, CO_2-storage.

1 Introduction

In the oil and gas production carbon dioxide corrosion may easily cause failure of pipelines [1–7] and this problem will become an issue when emission gasses are compressed from combustion processes into deep geological layers (CCS Carbon Capture and Storage) [8, 9]. Generally steels applied in pipeline

WIT Transactions on Ecology and the Environment, Vol 123, © 2009 WIT Press
www.witpress.com, ISSN 1743-3541 (on-line)
doi:10.2495/AIR090371

technology precipitate slow growing passivating $FeCO_3$-layers (siderite) [10–12, 26, 30, 31]. First CO_2 is dissolved to build a corrosive environment. Because the solubility of $FeCO_3$ in water is low (p_{Ksp} = 10.54 at 25°C [12, 13] a siderite corrosion layer grows on the alloy surface as a result of the anodic iron dissolution. In geothermal energy production the CO_2-corrosion is sensitively dependent on alloy composition, environmental conditions like temperature, CO_2 partial pressure, flow conditions and protective corrosion scales [10–23]. Engineering the geological CCS-site Ketzin, Germany, the first on-shore CO_2-storage (CO_2-SINK) no experience of the corrosion behaviour of the steels and therefore of the necessity to monitor the site was available for the aquifer water T=60°C / p=80 bar [24, 25] 40°C to 60°C). 60°C is a critical temperature region well known for severe corrosion processes [4, 6, 7, 19, 20, 26–29].

This work was carried out to predict the reliability of the on-shore CCS site at Ketzin, Germany and to get a better understanding of the corrosion behaviour of steels used for CO_2-injections.

2 Materials and methods

Exposure tests were carried out using samples made of thermal treated specimen of AISI 4140 (1%Cr) and AISI 420 (13%Cr) with 8 mm thickness and 20 mm width and 50 mm length. A hole of 3.9 mm diameter was used for sample positioning. The surfaces were activated by grinding with SiC-Paper down to 120 µm under water. Samples of each base metal were positioned within the vapour phase, the intermediate phase with a liquid/vapour boundary and within the liquid phase. The brine (as known to be similar to the Stuttgart Aquifer [32]: Ca^{2+}: 1760 mg/L, K^{2+}: 430 mg/L, Mg^{2+}: 1270 mg/L, Na^{2+}: 90,100 mg/L, Cl^{-}: 143,300 mg/L, SO_4^{2-}: 3600 mg/L, HCO^{3-}: 40 mg/L) was synthesized in a strictly orderly way to avoid precipitation of salts and carbonates. Flow control (2 NL/h) was done by a capillary meter GDX600_man by QCAL Messtechnik GmbH, München. The heat treatment of the samples between 700 h to 8000 h was disposed in a chamber kiln according to the conditions at the geological site at Ketzin/Germany at 60°C at 60 bar in an autoclave system and for reference at ambient pressure as well. X-ray diffraction was carried out in a URD-6 (Seifert-FPM) with CoKα-radiation with an automatic slit adjustment, step 0.03 and count 5 sec. Phase analysis was performed by matching peak positions automatically with PDF-2 (2005) powder patterns. Mainly structures that were likely to precipitate from the steels were chosen of the ICSD and refined to fit the raw-data-files using POWDERCELL 2.4 [33] and AUTOQUAN® by Seifert FPM.

Then the samples were embedded in a cold resin (Epoxicure, Buehler), cut and polished first with SiC-Paper from 180 µm to 1200 µm under water and then finished with diamond paste 6 µm and 1 µm. Different light optical and electron microscopy techniques were performed on specimens to investigate the layer structures and morphology of samples 60°C/700 h, 60°C/2000 h and 60°C/4000 h.

3 Results and discussion

3.1 Kinetics

Figure 1 illustrates the isothermal oxidation behaviour of the alloys AISI 420 X46Cr13 and AISI 4140 42CrMo-4 at 60°C/ambient pressure characterized by mass gain according to DIN 905 part 1-4.

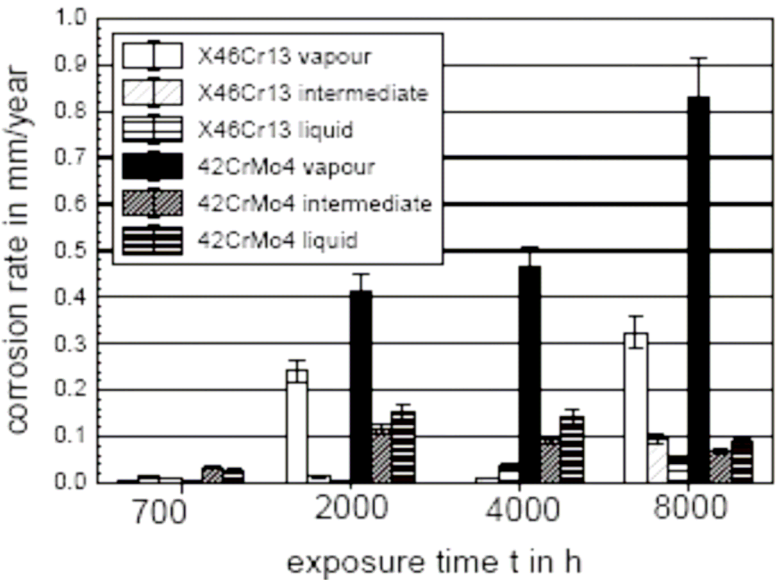

Figure 1: Corrosion rate as a function of heat treatment of the alloys X46Cr13 and 42CrMo-4 (60°C / CO_2 saturated brine / ambient pressure).

The greatest corrosion rates are found within the vapour phase, the lowest in the liquid phase. The high corrosion rates within the vapour phase are mainly due to the better access of CO_2 towards the sample surface in the water saturated CO_2-vapour phase. Samples in the intermediate phase show typical corrosion scale of the media they were exposed to but neither enhancement nor reduction of the corrosion rates were found. The greatest increase of the corrosion rates up to 2000 h is correlated to a passivating layer of siderite in CO_2-atmosphere. In general the corrosion rate increases with increasing CO_2 partial pressure [2], but in the presence of iron carbonate precipitates the corrosion rate may even decrease. This is the reason for the lower corrosion rates at longer exposure times with exception of the low Cr steel in the vapour phase. After 1 year of exposure (8000 h) there is an increase, which shows an extended reaction time and gives evidence of a change in mechanism.

After 700 h at 60 bar the results of corrosion rates are in good agreement with results at ambient pressure.

Pitting and shallow pit corrosion are only observed on the surface of the sample of X46Cr13 kept in the liquid phase with a maximum penetration depth of 4.6 mm after one year. This is nearly half of the pipe wall thickness (Figure 2). The time of heat treatment has little to no influence on the penetration depth of the pits, but significant influence on the number of counts [34–36].

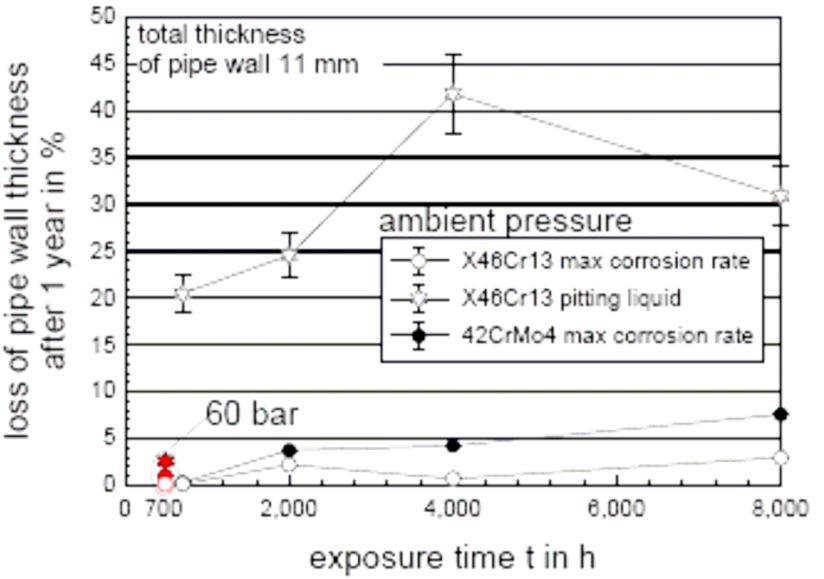

Figure 2: Corrosion rate as a function of heat treatment in CO2 saturated brine of the alloys X46Cr13 and 42CrMo-4 at 60°C at ambient pressure and at 60 bar.

3.2 Microstructure

3.2.1 AISI 4140, 42CrMo-4

Already after 700 h at ambient pressure as well as at 60 bar the 1% Cr alloy (AISI 4140) kept in the vapour phase shows a characteristic duplex corrosion layer (Figure 3). This comprises the outer corrosion layer, mainly consisting of siderite $FeCO_3$ and goethite α-FeOOH, and the inner layer mainly composed of siderite and spinel phase. Both layers contain mackinawite FeS and akaganeite $Fe_8O_8(OH)_8Cl_{1.34}$. The total layer thickness varies from 20 µm to 130 µm at ambient pressure and around 60 µm to 90 µm at 60 bar, where the inner layer shows elliptical islands of 10 µ to 30 µm. Samples in the intermediate phase show shallow pits with a depth about 50 µm and a width of 200 µm.

After 2000 h in the vapour phase the thickness of the outer layer various significantly but can rise up to 1.5 mm in the vapour phase and after 4000 h even a small inner layer is connected to 3-4 mm outer layer. Mainly consisting of the inner layer samples in the liquid phase have an inner layer altitude around 30 µm – 150 µm which grows in depth from 2000 h to 4000 h of heat treatment. Liquid phase samples do not show a typical inner corrosion layer.

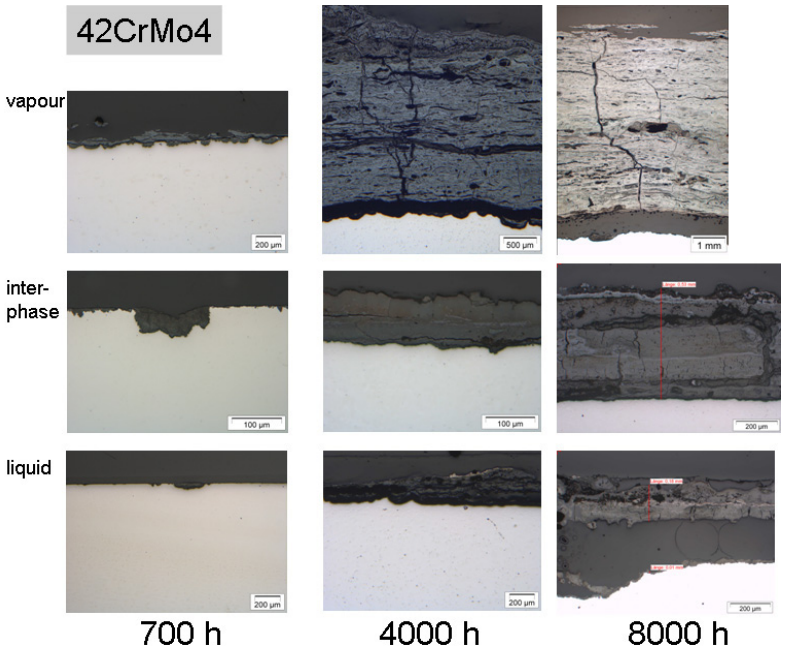

Figure 3: Cross section micrographs of 42CrMo-4 after heat treatment in CO_2 saturated brine at ambient pressure in saline aquifer water.

3.2.2 AISI 420, X46Cr13

As with the 1%Cr steel the 13% Cr steel X46Cr 13 shows surface corrosion with a typical duplex layer formation. Also the thickness of the corrosion layer in the vapour phase is much greater than in the intermediate and especially in the liquid phase. After 700 h at 60 bar and at ambient pressure there are islands of outer corrosion layers in the vapour and the intermediate phase that grow to 70 µm after 2000 h and even to 1.5 mm and a 500 µm inner layer after 4000 h while the liquid phase shows little to no surface corrosion (Figure 4).

While the outer layer mainly consists of siderite $FeCO_3$, goethite α-FeOOH and akaganeite $Fe_8O_8(OH)_8Cl_{1.34}$, the inner layer is composed of siderite, goethite and spinel phase. Mackinawite was not analysed. The carbides within the inner layer follow the stochiometric formula of me23C6 and are most likely manganese carbides.

The complicated multi-layered carbonate/oxide structure reveals siderite $FeCO_3$, with small amounts of Ca [10, 29] is goethite α-FeOOH, mackinawite FeS and spinelphases of various compositions as the main phases (Figures 5 and 6). Lepidocrocite γ-FeOOH and akaganeite $Fe_8O_8(OH)_8Cl_{1.34}$ are minor phases. Although carbides are not expected at these conditions Mn23C6 or some other not clearly stated composition may precipitate as followed from thermodynamic calculations (Software FACTSAGE®). In CO_2-environment precipitates on carbon steel may also consist of Fe_3C [12].

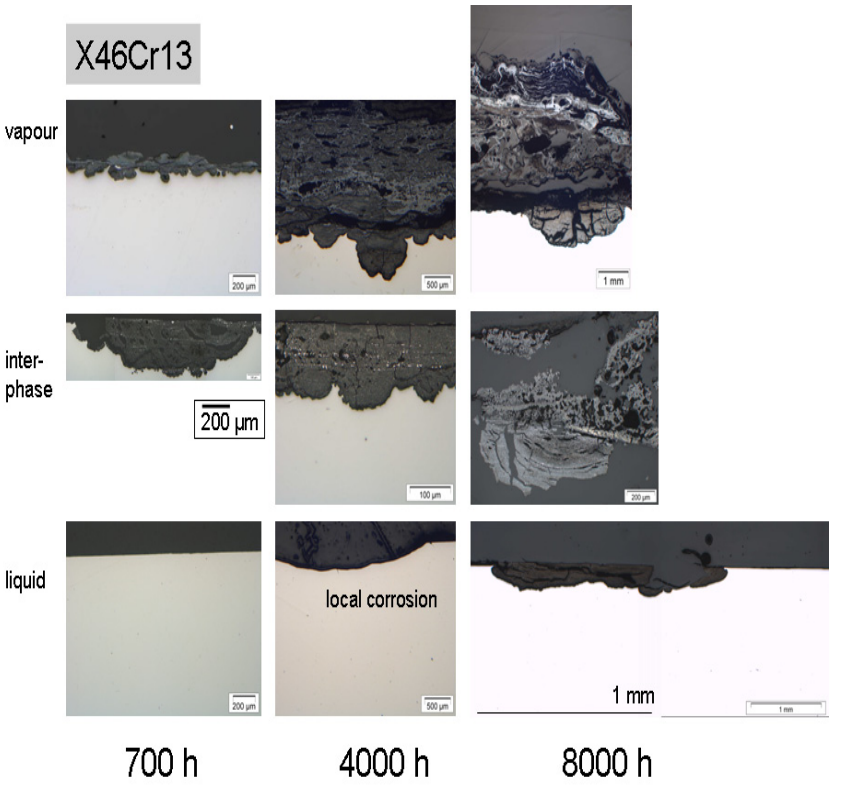

Figure 4: Cross section micrographs of X46Cr13 after heat treatment in CO_2 saturated brine at ambient pressure in saline aquifer water

The formation of the scale in geothermal water takes place in 2 steps as described in detail by Pfennig and Kranzmann [34, 35]. The first step may be attributed to the formation of Fe[II] compounds $FeOH_2$ [13]. The second step corresponds to the formation of a magnetite spinel type with Cr content in the 13% Cr steel and goethite and to the formation of siderite $FeCO_3$. Mackinawite FeS forms due to the saturation of the brine with H_2S and akaganeite $Fe_8O_8(OH)_8Cl_{1.34}$ due to the high salt content of the brine. Iron does not lead to a corrosion resistant stable oxygen film in O_2-free brine saturated with CO_2 at the presence of H_2S. Already little amounts of H_2S in geothermal water cause the change in mechanism of the iron corrosion in the H_2O-CO_2-system [13]. The strong adsorption of sulphide anions blocks the development of a protective oxide film. Therefore predominating phases are carbonates $FeCO_3$, hydroxides FeOOH and sulphides FeS. The further phase study including TEM-technique and the investigation of the combining reaction mechanism is a topic of future research project.

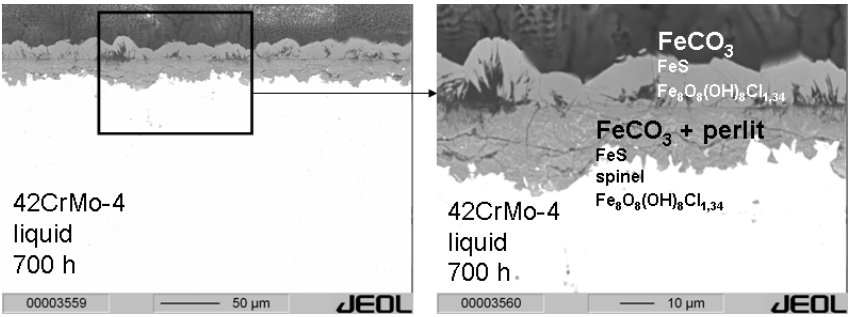

Figure 5: Cross section micrograph of 42CrMo-4 after 700 h of heat treatment in CO_2 saturated brine at ambient pressure in saline aquifer water.

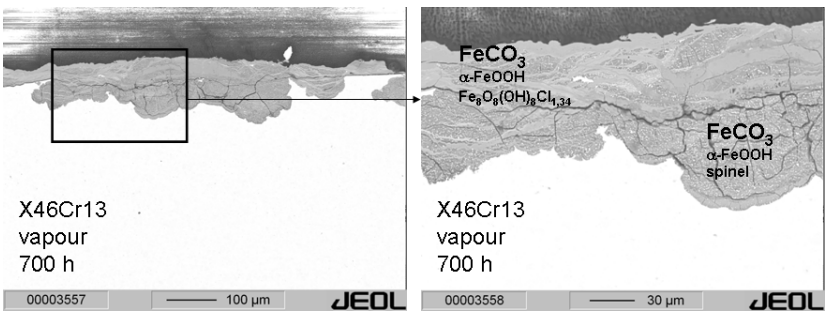

Figure 6: Cross section micrographs of X46Cr13 after 700 h of heat treatment in CO_2 saturated brine at ambient pressure in saline aquifer water.

4 Conclusion

The saturation of a geothermal brine with CO_2 leads to near linear corrosion rates for a 1% Cr (42CrMo-4) and 13%Cr (X46Cr13) steel. Highest surface corrosion rates are 0.8 mm/year (1% Cr) and 0.3 mm/year (13% Cr) in the vapour phase. The average intermediate and liquid corrosion rate for both type of steel is 0.1 mm/year. Severe pit corrosion with pit heights around 4.5 mm is only located on the X46Cr13 steel kept in the liquid where the gas flow and pressure is low. Main phase of the continuous scale is $FeCO_3$ siderite and FeS mackinawite in both types of steel. A complicated multi-layered carbonate/oxide structure reveals goethite α-FeOOH, lepidocrocite γ-FeOOH, spinelphases of various compositions and akaganeite $Fe_8O_8(OH)_8Cl_{1.34}$. In the high chromium-bearing alloy carbides ($Mn_{23}C_6$) are found. Since it is not clear whether the scales are protecting and therefore adhesive to the wall one should be aware of parts of the scale falling down into the injection pipe part. Following from these corrosion

rates the steels used for injecting technical CO_2 in Ketzin will withstand at least a 1 year period of injection without a need of replacement. if the tensile stresses can be reduced to a minimum and the decrease in pressure along the pipe wall thickness is kept low.

References

[1] L.S. Moiseeva and O.D. Kuksina, Material Science and Corrosion Protection – Predicting the Dorrosion Aggressiveness of CO_2-Containing Media in Oil and Gas Wells, Chemical and Petroleum Engineering, Vol. 36, No. 5-6, (307 – 311) 2000

[2] S. Nešić, "Key issues related to modelling of internal corrosion of oil and gas pipelines – A review", Corrosion Science 49 (2007) 4308–4338

[3] J.D. Drugli, T. Rogne, M. Svenning, S. Axelsen, The effect of buffered solutions in corrosion testing of alloyed 13% Cr martensitic steels for mildly sour applications, in: Proceedings of Corrosion/99, NACE International, Houston, TX, 1999, paper 99-586

[4] D.S. Carvalho, C.J.B. Joia, O.R. Mattos, Corrosion rate of iron and iron-chromium alloys in CO_2-medium, Corrosion Science 47 (2005) 2974-2986

[5] B.R. Linter, G.T Burstein, Reactions of pipeline steels in carbon dioxide solutions, Corrosion Science 41 (1999) 117-139

[6] M. Seiersten, Material selection for separation, transportation and disposal of CO_2, Corrosion paper no. 01042 (2001)

[7] R. Nyborg, Controlling Internal Corrosion in Oil and Gas Pipelines, Business Briefing: Exploration & Production: The Oil & Gas Review, issue 2 (2005) 70-74

[8] D.C. Thomas, Carbon Dioxide Capture for Storage in Deep Geologic Formations – Results from CO_2 Capture Project, Volume 1: Capture and Separation of Carbon Dioxide form Combustion Sources, CO_2 Capture Project, Elsevier Ltd UK 2005, ISBN 0080445748

[9] A.G. Reyes, W.J. Trompetter, K. Britten, J. Searle, Mineral deposits in the Rotokawa geothermal pipelines, New Zealand, Journal of Volcanology and Geothermal Research 119 (2002) 215-239

[10] Z.D. Cui, S.L. Wu, S.L. Zhu, X.J. Yang, Study on corrosion properties of pipelines in simulated produced water saturated with supercritical CO_2, Applied Surface Science 252 (2006) 2368-2374

[11] D.A. Lopez, W.H. Schreiner, S.R. de Sánchez, S.N. Simison, The influence of carbon steel microstructure on corrosion layers An XRS and SEM characterization, Applied Surface Science 207 (2003) 69-85

[12] D.A. Lopez, T. Perez, S.N. Simison, The influence of microstructure and chemical composition of carbon and low alloy steels in CO_2 corrosion. A state-of-the art appraisal, Materials and Design 24 (2003) 561-575

[13] J. Banaś, U. Lelek-Borkowska, B. Mazurkiewicz, W. Solarski, Effect of CO2 and H2S on the composition and stability of passive film on iron alloy in geothermal water, Electrochimica Acta 52 (2007) 5704-5714

[14] I. Thorbjörnsson, Corrosion fatigue testing of eight different steels in an Icelandic geothermal environment, Materials and Design Vol.16 No. 2 (1995) 97-102
[15] C. Bohne, Mikrostruktur, Eigenspannungs-zustand und Korrosionsbeständigkeit des kurzzeitlaserwärmebehandelten hochstick-stofflegierten Werkzeugstahls X30CrMoN15 1 Dissertation, Technische Universität Berlin 2000
[16] H. Gräfen, D. Kuron, Lochkorrosion an nichtrostenden Stählen, Materials and Corrosion 47, (1996), S.16
[17] http://www.ews-steel.com/pdf/vortrag_drvabe_06-11.pdf
[18] M. Kemp, A. van Bennekom, F.P.A. Robinson, Evaluation of the corrosion and mechanical properties of a range of experimental Cr-Mn stainless steels; Materials Science and Engineering A199 (1995) 183-194
[19] A. Tahara, T. Shinohara, Influence of the alloy element on corrosion morphology of the low alloy steels exposed to atmospheric environments, Corrosion Science 47 (2005) 2589-2598
[20] B. Brown, S. R. Parakala, S. Nesic, CO_2 corrosion in the presence of trace amounts of H_2S, Corrosion, paper no. 04736 (2004) 1-28
[21] R.M. Moreira, C.V. Franco, C.J.B.M. Joia, S. Giordana, O.R. Mattos, The effects of temperature and hydrodynamics on the CO_2 corrosion of 13Cr and 13Cr5Ni2Mo stainless steels in the presence of free acetic acid, Corrosion Science 46 (2004) 2987-3003
[22] T. Okazawa, T. Kobayashi, M. Ueda, T. Kushida, Development of super 13Cr stainless steel for CO_2 environment containing a small amount of H_2S, in: Proceedings of Corrosion/93, NACE Intern
[23] M. Ueda, A. Ikeda, Effect of Microstructure and Cr Content in Steel on CO_2 Corrosion, NACE Corrosion, paper no. 13 (1996) 1-6
[24] GeoForschungszentrum Potsdam, CO_2-SINK – drilling project, description of the project PART 1 (2006) 1-39
[25] http://www.co2sink.org/techinfo/drilling.htm
[26] H. Inaba, M. Kimura, H. Yokokawa, „ An analysis of the corrosion resistance of low chromium-steel in a wet CO_2-environment by the use of an electrochemical potential diagram, Corrosion Science 38 (1996) 1449-1461
[27] JFE Steel Corporation – Pipes and Tubes – OCTG, http://www.jfesteel.co.jp/en/products/pipes/octg/index.html
[28] S.L Wu, Z.D. Cui, G.X. Zhao, M.L. Yan, S.L. Zhu, X.J. Yang, EIS study of the surface film on the surface of carbon steel form supercritical carbon dioxide corrosion", Applied Surface Science 228 (2004) 17-25
[29] T. Kamimura, M. Stratmann, "The influence of chromium on the atmospheric corrosion of steel", Corrosion Science 43 (2001) 429-447
[30] J. Carew, S. Akashah, "Prediction techniques for materials performance in the crude oil production system", Modelling Simulation, Material Science Engineering 2 (1994) 371-382

[31] S.L Wu, Z.D. Cui, F. He, Z.Q. Bai, S.L. Zhu, X.J. Yang, Characterization of the surface film formed from carbon dioxide corrosion on N80 steel, Materials Letters 58 (2004) 1076-1081

[32] A. Förster, B. Norden, K. Zinck-Jørgensen, P. Frykman, J. Kulenkampff, E. Spangenberg, J. Erzinger, M. Zimmer, J. Kopp, G. Borm, C. Juhlin, C. Cosma, S. Hurter, 2006, Baseline characterization of the CO2SINK geological storage site at Ketzin, Germany: Environmental Geosciences, V. 13, No. 3 (September 2006), pp. 145-161.

[33] SW. Kraus and G. Nolze, POWDER CELL – a program for the representation and manipulation of crystal structures and calculation of the resulting X-ray powder patterns, J. Appl. Cryst. (1996), 29, 301-303

[34] Pfennig, A., Kranzmann, A., "Influence of CO_2 on the corrosion behaviour of 13Cr martensitic stainless steel AISI 420 and low alloyed steel AISI 4140 exposed to saline aquifer water environment", Intl. Conference on Environment 2008 ICENV 2008, Penang, Malaysia, December 15th to 17th, 2008

[35] Pfennig, A., Kranzmann, A., "Effects of Saline Aquifere Water on the Corrosion Behaviour of Injection Pipe Steels 1.4034 and 1.7225 during Exposure to CO_2 Environment", Green House Gas Emission Reduction Technologies GHGT9 Conference, Washington DC, USA, November 16th to 20th, 2008

[36] Pfennig, A., Kranzmann, A., "Effect of CO_2 on the stability of steels with 1% and 13% Cr in saline water", Water, Steam and Aqueous Solutions – Advances in Science and Technology of Power Generation, ICPWS XV, 15th, Berlin, September 8-11, 2008